Simulated Seismic-Load Tests on Full-Scale Five-Story Masonry Building

By F. Seible,[1] Member, ASCE, G. A. Hegemier,[2] A. Igarashi,[3] and G. R. Kingsley,[4] Member, ASCE

Abstract: The first U.S. full-scale five-story building test under simulated seismic loads was conducted at the University of California, San Diego. The full-scale reinforced masonry (RM) research building consisted of coupled, flanged, fully grouted concrete masonry walls and precast prestressed hollow-core plank floors with reinforced-concrete topping. The seismic-simulation tests were conducted under the direction of the Technical Coordinating Committee for Masonry Research (TCCMAR) to validate new analysis and design models for masonry buildings in seismic zones. The complete seismic simulation testing of the five-story structural wall building under recorded earthquake ground-motion segments was possible through soft coupling between the loading system and the stiff test structure, and improvements to the on-line actuator-control algorithm as part of the implicit time-integration scheme. The development and implementation of the generated sequential displacement (GSD) procedure for the experimental multidegree-of-freedom seismic-load simulation is described and illustrated by detailed examples of responses.

INTRODUCTION

Extensive damage to unreinforced masonry buildings in past earthquakes has severely limited the use of masonry construction in seismic zones despite significant advances in providing ductility through the use of steel reinforcement. To overcome perceived seismic performance deficiencies of masonry construction, the U.S. Coordinated Program for Masonry Building Research was initiated in the mid 1980s under the auspices of the U.J.N.R. (United States–Japan Cooperative Agreement on Natural Resources), with the primary objective of developing new design criteria for reinforced masonry (RM) buildings in seismic zones. Twenty-eight coordinated research tasks were conducted in the United States under the direction of the U.S. Technical Coordinating Committee for Masonry Research (TCCMAR/US) to develop analysis and design models, fully sponsored and verified through experimental testing, to predict the complete response of RM buildings in seismic zones (Noland 1990). As the final experimental validation of the TCCMAR/US design philosophy and analytical models, a full-scale five-story RM research building (see Figs. 1 and 2) was tested under simulated seismic loads at the University of California, San Diego. Although prior TCCMAR experimental tasks characterized the behavior of individual structural ma-

[1]Prof. of Struct. Engrg., Dept. of Appl. Mech. and Engrg. Sci., Univ. of California, San Diego, La Jolla, CA 92093-0411.

[2]Prof. of Appl. Mech., Dept. of Appl. Mech. and Engrg. Sci., Univ. of California, San Diego, La Jolla, CA.

[3]Grad. Res. Asst., Dept. of Appl. Mech. and Engrg. Sci., Univ. of California, San Diego, La Jolla, CA.

[4]Grad. Res. Asst., Dept. of Mech. and Engrg. Sci., Univ. of California, San Diego, La Jolla, CA.

Note. Discussion open until August 1, 1994. Separate discussions should be submitted for the individual papers in this symposium. To extend the closing date one month, a written request must be filed with the ASCE Manager of Journals. The manuscript for this paper was submitted for review and possible publication on February 1, 1993. This paper is part of the ***Journal of Structural Engineering***, Vol. 120, No. 3, March, 1994. ©ASCE, ISSN 0733-9445/94/0003-0903/$2.00 + $.25 per page. Paper No. 5534.

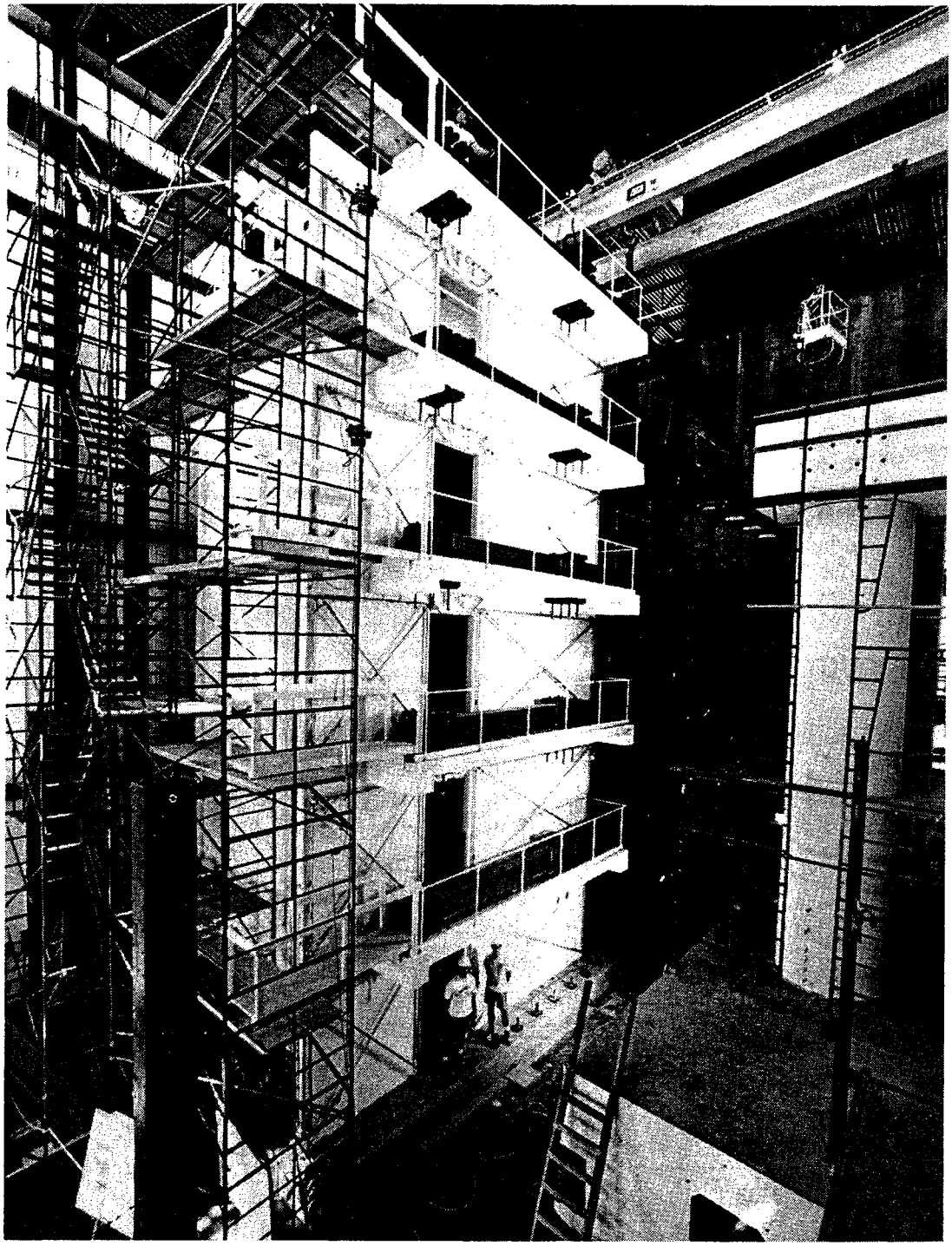

FIG. 1. Full-Scale Five-Story RM Research Building

sonry components and subassemblages, the five-story research building test allowed the investigation of a complete full-scale structural system, including the complex interaction of components and subsystems.

The three principal objectives for the RM research building test were: (1) To provide a test bed for the developed TCCMAR seismic design philosophy; (2) to provide benchmark data for the calibration and verification of TCCMAR analysis models; and (3) to advance the state of the art in full-scale laboratory testing of stiff multidegree-of-freedom (MDOF) structures under simulated seismic loads. To test the full-scale five-story research building under simulated seismic loads rather than under an increasing cyclic, fixed lateral load distribution, a generated sequential displacement (GSD) test procedure was developed. The GSD test method combines character-

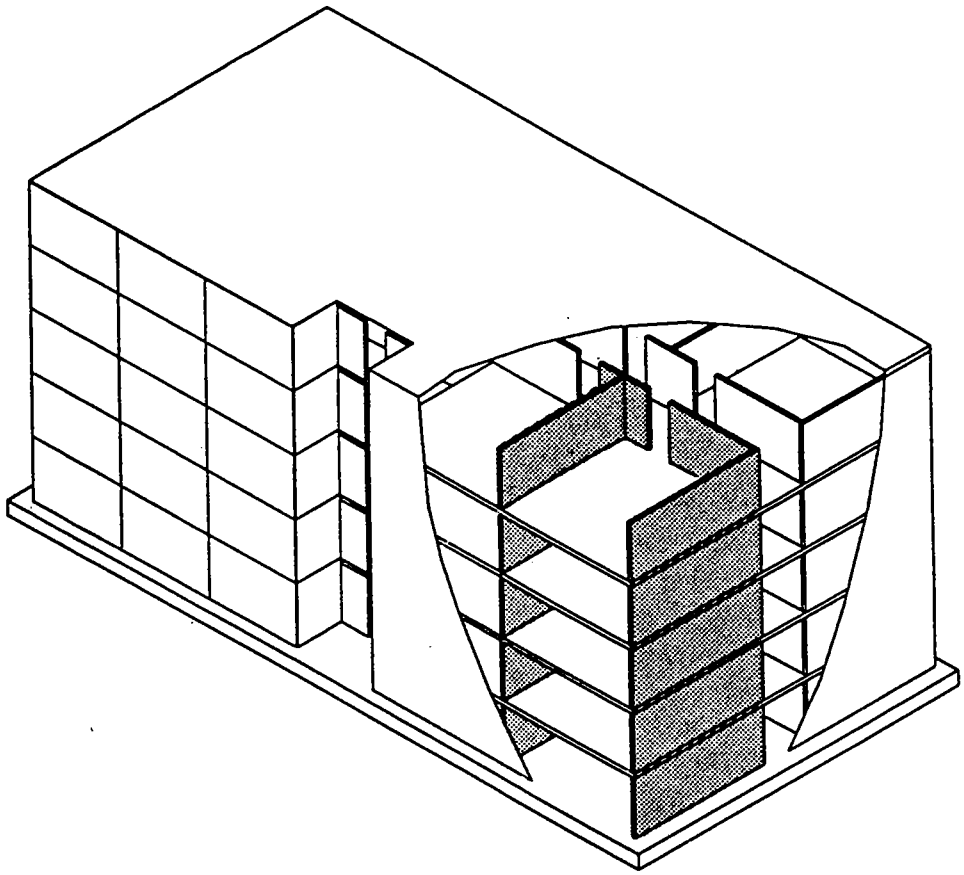

FIG. 2. Prototype for RM Research Building

istics of the sequential phased displacement procedure developed under TCCMAR (Porter 1987) and pseudodynamic or on-line test principles (Mahin et al. 1989; Takanashi and Nakashima 1987). The idea of a sequentially phased displacement input pattern of controlled increasing magnitude is maintained, while the distribution of simulated seismic forces or lateral loads is determined pseudodynamically from selected ground motion input segments and the current stiffness characteristics of the test building. Ground-motion input segments are selected to exercise the structure through progressively increasing damage or limit states. The response of the structure to a complete recorded ground motion is not sought, nor is it necessary, because the use of capacity design principles decreases the sensitivity of the structural response to specific ground motions (Paulay and Priestley 1992). Key advantages of this GSD testing procedure are that: (1) All damage to the test structure is inflicted under natural load distribution patterns; (2) critical behavior and design limit states can be sequentially studied; and (3) possible inherent higher-mode effects can be captured.

To test a stiff full-scale structural wall building from its initial undamaged state under simulated seismic loads, modifications and improvements to conventional pseudodynamic test procedures were necessary, both in the on-line control algorithms and in the physical load introduction and distribution throughout the stiff multidegree-of-freedom (MDOF) test structure. A detailed description of the development and implementation of the simulated seismic-load testing procedure is presented together with predicted and experimentally observed response examples. The seismic response evaluation of the five-story RM building and the validation of TCCMAR analysis and design models are discussed in a companion paper (Seible et al. 1994).

RESEARCH BUILDING, TEST SETUP, AND LOADING SYSTEM

To discuss the simulated seismic-load test procedure, a description of the research building, the test setup and the loading system is required, as well as a definition of the earthquake ground-motion input sequence, which allowed the experimental response verification at characteristic design and behavior limit states of the five-story RM research building.

The seismic-load resistance was provided by two flanged walls, one short wall with a mid-side or T flange and a long wall with an end or L flange, as shown in Fig. 3, coupled by a floor system consisting of six precast prestressed topped hollow-core planks. The overall dimensions of the full-scale research building are depicted in Fig. 3 with a building height of five at 2.6 m = 13.2 m (five at 8 ft 8 in. = 43 ft 4 in.) and a plan dimension of 7. 3 × 6.1 m (24 ft × 20 ft). The lateral or seismic-load application system consisted of 10 servocontrolled hydraulic actuators in pairs of two per floor level at five discrete degrees of freedom (DOF), as schematically shown by actuators 1 through 10 in Fig. 3. The two actuators per floor level were required for control of the torsional mode, which is not present in the prototype building, see Fig. 2. Since correct seismic-load simulation on the five-story building should be mass proportional, it is reasonable to introduce loads at the floor levels, where a natural mass concentration in a building exists. To distribute the lateral forces across the plan floor area, stiff load-distribution beams (W18 × 97) were used and connected to the floor system by means of 12.7 mm (1/2 in.) thick elastomeric pads to provide uniform load distribution between the two load points. The actual force transfer between the floor slab and the elastomeric pads was by means of a friction connection provided by four external high-strength bars, which clamped the load beam to the floor slab with a normal force of approximately 224 kN (50 kip) per pad. In addition to the uniform load distribution these elastomeric pads provided a reduced apparent stiffness or soft coupling of the MDOF system, reducing the tendency of the servocontrolled actuators to counteract each other in a spurious higher-mode response. The soft coupling between the loading system and the test structure also provided displacement amplifications for the active actuator control, particularly in the initial stiff structural state, allowing a structural displacement error control smaller than the actuator displacement precision, as derived in (Igarashi et al. 1992). Furthermore, the elastomeric pads allowed for limited unconstrained structural rotations and expansions, and their soft coupling protected the research building against actuator instabilities during the shakedown testing.

SIMULATED SEISMIC-LOAD HISTORY AND TEST PROGRAM

One of the objectives of the full-scale test was to use only simulated seismic load/displacement segments to exercise the research building to new response limit states. Sequential behavior limit states to be achieved with the GSD procedure were the initial uncracked state, first cracking in the walls and floor slabs, first yield in the walls and floor slabs, the formation of a global plastic mechanism and the ultimate limit state of wall toe crushing or lateral capacity degradation. Earthquake ground-acceleration records from the 1971 San Fernando earthquake (M_s = 6.6, thrust fault) and the 1979 Imperial Valley earthquake (M_s = 6.8, strike slip fault) were used for the GSD load input. Windows from six acceleration records from the aforementioned events were selected and slightly scaled as shown in Table 1 to match the UBC S2 design spectra over a period range from 0.2 to 0.6-sec,

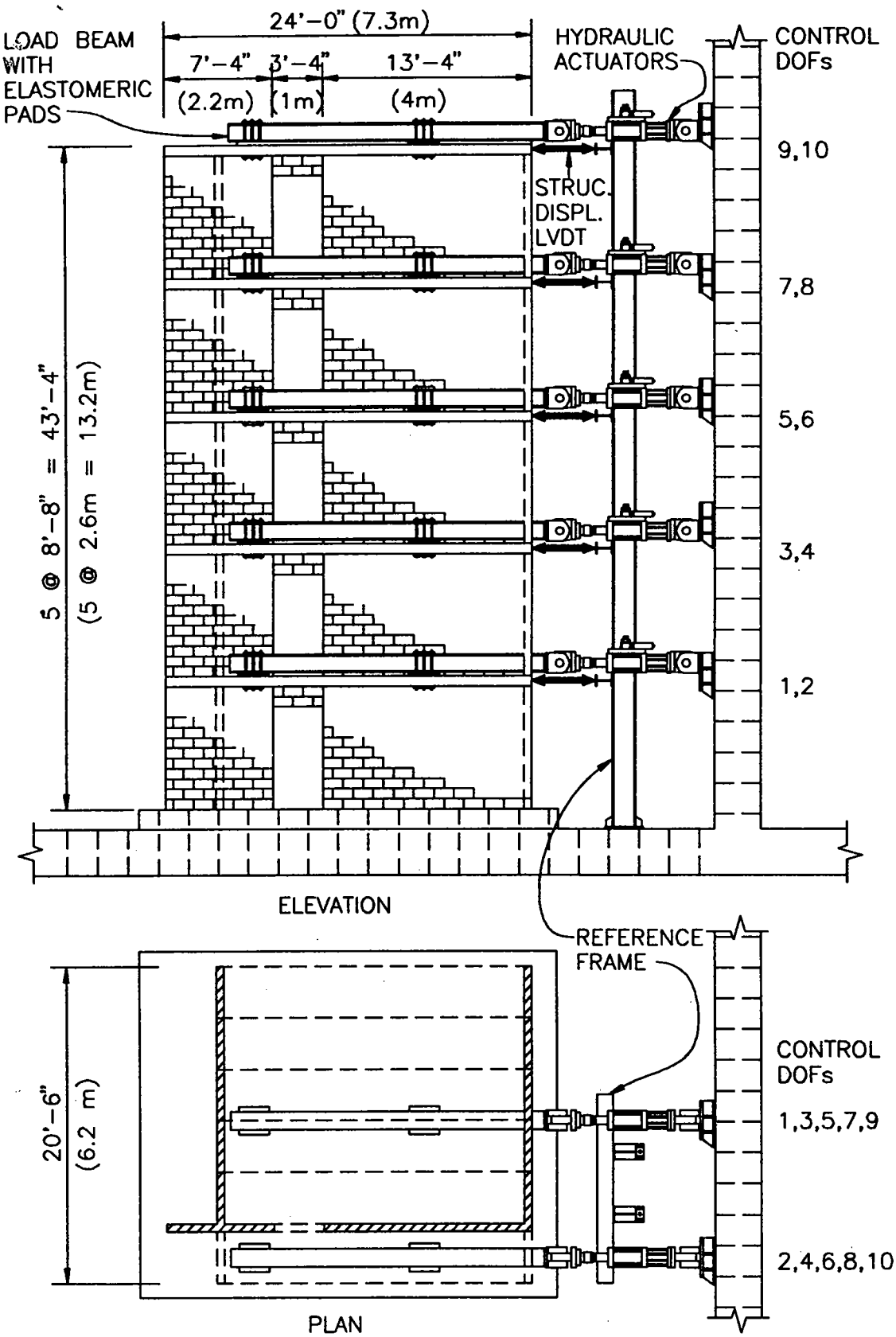

FIG. 3. Plan and Elevation of the Research Building and Test Setup

which was the expected fundamental response range of the test structure. Utilizing appropriate initial conditions determined analytically from the complete ground-motion records for the front end of these earthquake windows, a series of 15 ground-acceleration segments ranging in duration from 1 to 3 sec was applied sequentially to the research building resulting in a combined 25 sec earthquake record, as shown in Fig. 4, to obtain target

TABLE 1. Summary of Earthquake Record Windows

Recorded (1)	Test number (2)	Acceleration record (3)	Window (4)	Duration (sec) (5)	Scale factor (6)	Peak acceleration (g) (7)	Time step (sec) (8)
1	31	Pine Union School	8.15–9.16	1.01	0.10	0.03	0.005
1	35	Brockman Road	4.95–5.96	1.01	1.50	0.11	0.005
1	39	Brockman Road	4.95–6.95	2.00	1.23	0.10	0.010
2	42	Anderson Road	3.90–5.96	2.06	−1.50	0.31	0.010
2	46	Brawley Airport	6.18–8.20	2.02	−1.08	0.24	0.020
2	49	Hollywood Storage P.E. Lot	2.00–4.04	2.04	1.00	0.21	0.010
2	53	Pine Union School	8.15–9.15	1.00	0.75	0.20	0.010
2	54	Pine Union School	8.15–10.08	1.93	1.00	0.27	0.010
2	58	Brawley Airport	6.18–6.87	0.69	1.00	0.12	0.010
3	59	Brawley Airport	6.18–6.86	0.68	−1.20	0.15	0.010
3	60	Brawley Airport	6.18–7.35	0.17	−1.25	0.23	0.010
3	61	Brawley Airport	6.18–8.63	2.45	−1.40	0.31	0.010
3	64	Anderson Road	3.90–6.83	2.93	1.10	0.54	0.010
4	68	Anderson Road	3.90–5.73	1.83	−1.40	0.69	0.010
4	71	Anderson Road	3.90–5.54	1.64	1.70	0.84	0.010

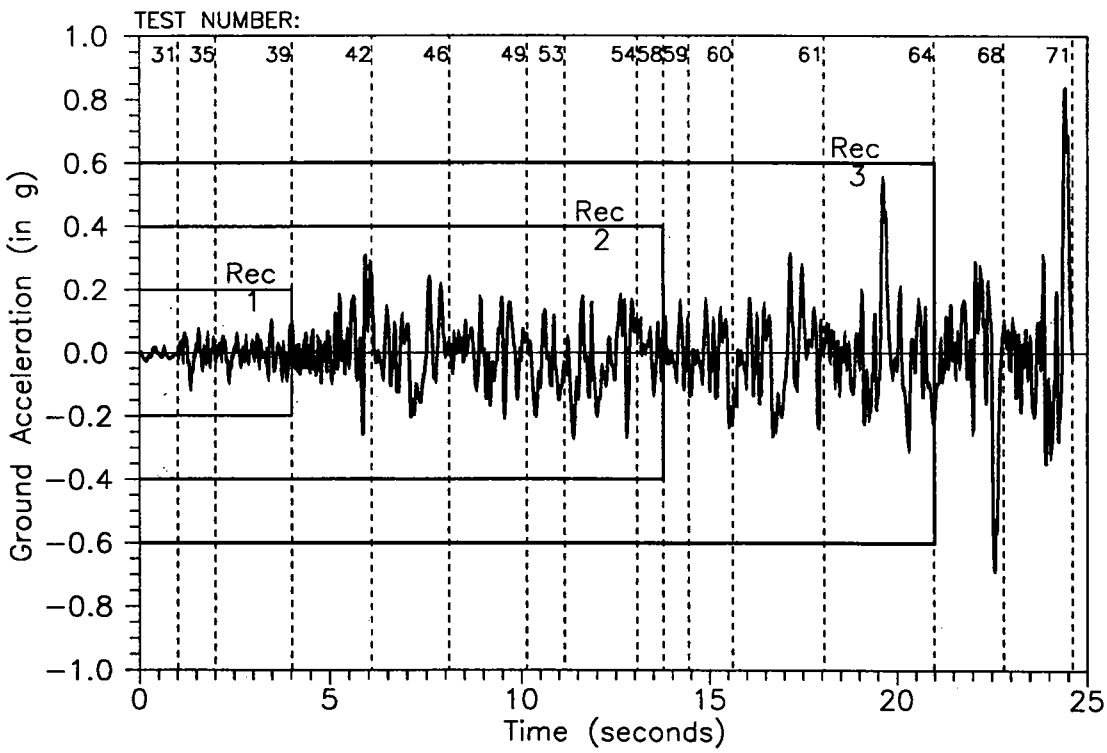

FIG. 4. Generated Sequential Earthquake Record for Five-Story Building Test

response displacements that increase in magnitude and correspond to the foregoing outlined design and behavior limit states. The acceleration-response spectra for different ground-motion segments as indicated in Fig. 4 are depicted in Fig. 5 together with scaled UBC S2 design spectra levels.

Results from MDOF GSD tests are typically not in a form in which they can be used in direct comparison with conventional equivalent lateral load design models, particularly when higher-mode effects contribute to the seismic response. With higher-mode contributions the ratio of overall building overturning moment to base shear is not constant resulting in base shear versus displacement hysteresis plots, which are not the usual smooth hysteresis loops obtained from cyclic tests under fixed design load (i.e. inverse

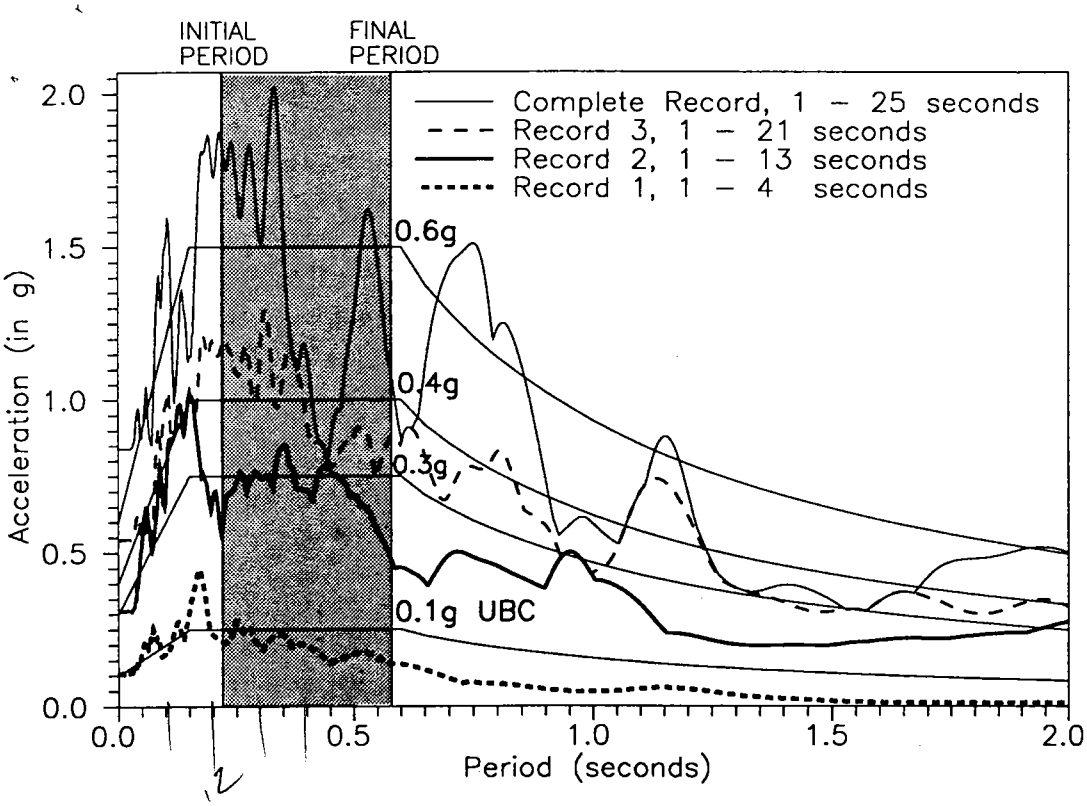

FIG. 5. Acceleration Response Spectra (5% Damping) for Four Windows from Generated Sequential Earthquake Record

triangular) distributions. Thus, to compare the RM research building response directly to inverse triangular design load models, each GSD segment was followed by an inverse triangular load (ITL) test to the same overall building-drift level as previously recorded during the GSD test. In this way, for a test structure with predominantly first-mode response, all significant damage will be introduced during the GSD phase; and important design information can be deducted from the subsequent ITL test. Each GSD and ITL sequence was followed by a modal low-level stiffness measurement to obtain an updated stiffness matrix to be used for constant stiffness iterations during the GSD procedure to be described in the following.

SIMULATED SEISMIC-LOAD TEST DEVELOPMENT

The three outlined procedures (GSD, ITL, and stiffness measurement) all require a similar algorithm for displacement control of the test structure. Therefore, prior to a description of each of the test procedures, common aspects of the on-line control will be presented.

On-Line Displacement Control

To apply a prescribed set of displacement conditions to a stiff five-story structure at 10 independent locations through soft elastomeric pads requires some special considerations in the on-line displacement control algorithms developed for MDOF systems (Shing et al. 1991). In the following discussion let n_s be the number of structural control locations (actuators), and $\hat{\mathbf{x}}_S^{(k)}$ and $\hat{\mathbf{r}}_S^{(k)}$ be the corresponding n_s-dimensional measured ($\hat{}$) displacement and restoring force vectors at iteration step k, respectively. For the five-story RM research building, $n_s = 10$ as shown in Fig. 3. It can be shown that $\hat{\mathbf{x}}_S^{(k)}$ ($k = 0, 1, \ldots$) converges to the specified target displacement $\mathbf{x}_{S\text{target}}$ if the actuator displacement for the next iteration, $\mathbf{x}_a^{(k+1)}$, is determined by

$$\mathbf{x}_a^{(k+1)} = \mathbf{x}_a^{(k)} + \mathbf{N}[\mathbf{x}_{Starget}^{(k)} - \hat{\mathbf{x}}_S^{(k)}]; \qquad k = 0, 1, \ldots \quad \ldots\ldots\ldots\ldots\ldots (1)$$

where $\mathbf{N}$ = a scaling matrix of dimension $n_s \times n_s$. The implementation of the implicit time-integration scheme in the GSD algorithm requires that the target displacement $\mathbf{x}_{Starget}$ be updated at every iteration step (k), thus it is notated $\mathbf{x}_{Starget}^{(k)}$ in (1). The scaling matrix $\mathbf{N}$ controls convergence, and permits convergence acceleration when estimated or measured stiffness values for the test structure and the elastomeric pads are used (Igarashi et al. 1992). For the five-story RM building tests, $\mathbf{N}$ is constructed from several terms and factors, as shown in the following expression:

$$\mathbf{N} = \nu\mathbf{P}\left[\mathbf{N}_r + \mathbf{R}_d\left(\mathbf{N}_d + \frac{1}{\kappa_p}\mathbf{A}\hat{\mathbf{K}}\mathbf{A}^+\right)\right] \quad \ldots\ldots\ldots\ldots\ldots\ldots\ldots (2)$$

Each term in (2) represents a specific aspect of convergence. The scalar ν is a global scaling factor, and $\mathbf{P}$ represents the "torsion filtering" required to suppress the tendency of the test structure to position itself on opposite sides of the tolerance band provided for the n_s structural displacements, caused by the accumulation of displacement measurement errors associated with strict torsion control. The matrix $\mathbf{N}_r$ controls the convergence of the rotational (torsional) displacements; $\mathbf{R}_d$ is a convergence acceleration matrix and the scalar κ_p is a parameter related to the coupling between the load beam and the structure. The matrix $\mathbf{N}_d$ is the general translational convergence control matrix, and the matrix $\mathbf{A}$ is described later. The matrix $\hat{\mathbf{K}}$ is the previously measured initial stiffness matrix of the test structure (see following description of modal stiffness measurement), which was replaced by a continuously updated tangent stiffness matrix for the GSD tests in inelastic range. Details on these parameters are provided elsewhere (Igarashi 1993).

If torsional displacements are not allowed, the two structural displacements at each floor are constrained to be equal, thus reducing the problem from an n_s-dimensional problem to an n-dimensional problem, where n represents the five active floor translational displacement DOF. The n_s-dimensional structural target displacement vector $\mathbf{x}_{Starget}$ may be obtained from the n-dimensional floor-level-displacement vector $\mathbf{x}_{target}$ by means of an $n_s \times n$ transformation matrix $\mathbf{A}$ in the form of

$$\mathbf{x}_{Starget} = \mathbf{A}\mathbf{x}_{target} \quad \ldots\ldots\ldots\ldots\ldots\ldots\ldots\ldots\ldots\ldots\ldots\ldots\ldots\ldots\ldots (3)$$

The measured structural restoring force vector $\hat{\mathbf{r}}_S^{(k)}$ and the structural displacement vector $\hat{\mathbf{x}}_S^{(k)}$ are then related to the floor level DOF restoring force and displacement vectors as

$$\mathbf{r}^{(k)} = \mathbf{A}^T\hat{\mathbf{r}}_S^{(k)} \qquad k = 0, 1, \ldots \quad \ldots\ldots\ldots\ldots\ldots\ldots\ldots\ldots\ldots\ldots (4a)$$

$$\hat{\mathbf{x}}^{(k)} = \mathbf{A}^+\hat{\mathbf{x}}_S^{(k)} \qquad k = 0, 1, \ldots \quad \ldots\ldots\ldots\ldots\ldots\ldots\ldots\ldots\ldots\ldots (4b)$$

where the transformation matrix $\mathbf{A}$ and its pseudoinverse, $\mathbf{A}^+$, can be written as

$$\mathbf{A} = \begin{bmatrix} 1 & & & & 0 \\ 1 & & & & \\ & 1 & & & \\ & 1 & & & \\ & & 1 & & \\ & & 1 & & \\ & & & 1 & \\ & & & 1 & \\ 0 & & & & 1 \\ & & & & 1 \end{bmatrix} \quad \text{(5a)}$$

$$\mathbf{A}^{+} = (\mathbf{A}^T\mathbf{A})^{-1}\mathbf{A}^T = \begin{bmatrix} \frac{1}{2}\ \frac{1}{2} & & & & 0 \\ & \frac{1}{2}\ \frac{1}{2} & & & \\ & & \frac{1}{2}\ \frac{1}{2} & & \\ & & & \frac{1}{2}\ \frac{1}{2} & \\ 0 & & & & \frac{1}{2}\ \frac{1}{2} \end{bmatrix} \quad \text{(5b)}$$

Thus, the displacement DOF at each floor is defined by the average of the two measured displacements at each level, and the floor restoring force is the sum of the forces in the two actuators at each level. The response quantities in (4) are then used to control the five floor DOFs.

Generated Sequential Displacement Procedure

As just outlined, the GSD testing procedure developed to test the full-scale five-story research building is directly based on pseudodynamic testing principles, which can be applied in cases where full-scale shake-table testing is not feasible or where response studies in pseudotime are advantageous to obtain data at rates that allow in-test modifications. Conventional explicit time-integration schemes frequently used in pseudodynamic tests require for numerical stability a short time interval, which is determined by the natural period of the highest mode. Such excessively small time intervals can result in extremely small displacement increments beyond the performance limits of the actuator control, in turn causing large restoring-force errors. To overcome these problems the presented GSD developments are based on the implicit Hilber α method as proposed by Shing et al. (1991), which can be summarized as follows:

$$\mathbf{Ma}(i+1) + (1+\alpha)\mathbf{Cv}(i+1) - \alpha\mathbf{Cv}(i) + (1+\alpha)\mathbf{r}(i+1) - \alpha\mathbf{r}(i) = (1+\alpha)\mathbf{f}(i+1) - \alpha\mathbf{f}(i) \quad \text{(6)}$$

$$\mathbf{x}(i+1) = \mathbf{x}(i) + \Delta t\mathbf{v}(i) + \Delta t^2\left[\left(\frac{1}{2} - \beta\right)\mathbf{a}(i) + \beta\mathbf{a}(i+1)\right] \quad \text{(7)}$$

$$\mathbf{v}(i+1) = \mathbf{v}(i) + \Delta t[(1-\gamma)\mathbf{a}(i) + \gamma\mathbf{a}(i+1)]; \qquad i = 0, 1, \ldots \quad \text{(8)}$$

where $\mathbf{M}$ = mass matrix; $\mathbf{C}$ = damping matrix; $\mathbf{x}(i)$ = displacement vector at the time step i; $\mathbf{v}(i)$ = velocity vector at the time step i; $\mathbf{a}(i)$ = acceleration vector at the time step i; $\mathbf{r}(i)$ = restoring force vector at the time step i; $\mathbf{f}(i)$ = excitation force vector at the time step i; Δt = integration time interval; and α, β, γ = scalar integration constants.

In principle, an implicit scheme in the pseudodynamic test requires that the restoring force at the next step be obtained in order to calculate the

next target displacement. For the GSD procedure, the on-line displacement control just described was incorporated into the implementation of the Hilber α method proposed by Shing et al. (1991) updating the target displacement at each iteration step based on the measured displacement and calculated restoring-force error. A complete flowchart for the GSD algorithm is depicted in Fig. 6. The major difference in the developed procedure from the algorithm proposed by Shing et al. is the control of the loading system with elastomeric pads, and a reduced number of DOFs in the numerical time-integration scheme as a result of the no-torsion requirement to the test structure. The procedure illustrated in Fig. 6 consists of two control loops: the inner control loop and the outer control loop. Each inner loop cycle at iteration k performs: (1) Measurement of the current displacement and restoring force; (2) calculation of the updated target displacements in accordance with the implicit time integration scheme; and (3) determination of the appropriate actuator displacement command using the on-line displacement control algorithm described earlier. When the measured structural displacement and the calculated target displacement are within a specified error tolerance, the convergence of both translational and rotational displacements is assumed to be satisfied, and the next outer loop cycle (integration time step i) is carried out. When the acceleration, velocity, and displacement vectors are computed at the end of the outer loop, the measured restoring force vector is modified using the initial stiffness matrix and this corrected restoring force vector is used in the calculation at the next time step. Also, the estimated tangent stiffness matrix used in the scaling matrix is continuously updated using the measurements of the displacement and restoring force in each outer loop cycle (Igarashi 1993).

Inverse Triangular Load Test Control

To impose an inverse triangular load distribution pattern in displacement control to the five-story test structure requires actuator-displacement command signals that will result in the prescribed restoring-force pattern. Displacement control of the actuators is necessary to control torsion. The ITL algorithm assumes that $x^{(k+1)}$ is the floor-level-displacement vector that satisfies the conditions

$$\mathbf{e}_n^T\mathbf{x}^{(k+1)} = x_{\text{top}} \quad \text{(9)}$$

$$\hat{\mathbf{K}}[\mathbf{x}^{(k+1)} - \hat{\mathbf{x}}^{(k)}] + \hat{\mathbf{r}}^{(k)} = \alpha^{(k+1)}\mathbf{u}; \qquad k = 0, 1, \ldots \quad \text{(10)}$$

where $\hat{\mathbf{K}}$ = measured initial stiffness matrix; $\alpha^{(k+1)}$ = an unknown scalar; x_{top} = specified maximum top displacement obtained in the previous GSD test; $\mathbf{u} = \{1, 2, 3, 4, 5\}^T$, representing the inverse triangular load pattern; and $\mathbf{e}_n^T = \{0, 0, 0, 0, 1\}$ = a unit vector. Thus, (9) and (10) specify that the new displacement vector $\mathbf{x}^{(k+1)}$ has the specified top displacement, and that if $\mathbf{x}^{(k+1)}$ is applied the restoring force is proportional to the inverse triangular load pattern provided that $\hat{\mathbf{K}}$ coincides with the actual structural stiffness. By rearranging the terms of (9) and (10) to separate the unknowns $\mathbf{x}^{(k+1)}$ and $\alpha^{(k+1)}$, a set of simultaneous linear equations is obtained

$$\begin{bmatrix} \hat{\mathbf{K}} & -\mathbf{u} \\ \mathbf{e}_n^T & 0 \end{bmatrix} \begin{Bmatrix} \mathbf{x}^{(k+1)} \\ \alpha^{(k+1)} \end{Bmatrix} = \begin{Bmatrix} \hat{\mathbf{K}}\hat{\mathbf{x}}^{(k)} - \hat{\mathbf{r}}^{(k)} \\ x_{\text{top}} \end{Bmatrix} \quad \text{(11)}$$

The calculated displacement vector $\mathbf{x}^{(k+1)}$ is used as the target displacement in the on-line displacement control algorithm described above, and this

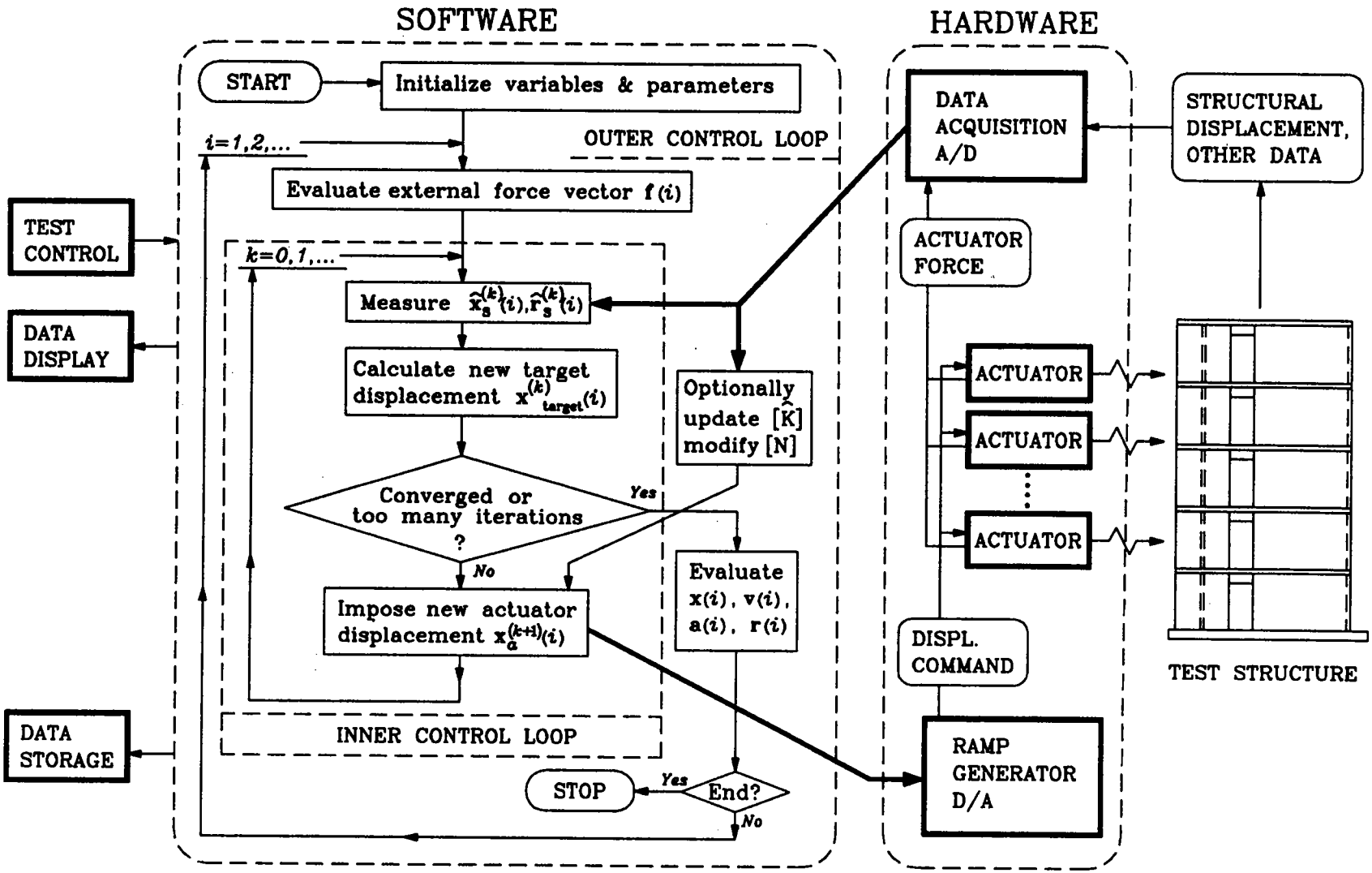

FIG. 6. Control Algorithm Flowchart for GSD Tests

target displacement is updated in each iteration step based on the displacement and load measurements as outlined in the inner loop of the GSD algorithm in Fig. 6. The iteration process is repeated until the calculated displacement increment falls within the specified displacement error tolerance. The overall structural target top displacement from the GSD test is subdivided into 40 or more load steps in the form of an outer control loop which makes the ITL algorithm flowchart very similar to the one presented in Fig. 6 for the GSD tests.

Modal Stiffness Measurements

Estimates of the stiffness matrix for small displacement levels were obtained experimentally after each GSD and ITL sequence to get a new initial stiffness matrix for the GSD and ITL iterations, and to make a linear elastic prediction of the displacement response for the next earthquake ground-motion input. The stiffness matrix of the five-story building was measured by imposing five independent displacement patterns to the structure, and multiplying the inverse of the deformation pattern matrix by the obtained restoring-force matrix. The five natural vibration mode shapes were chosen as the independent displacement patterns, and these were applied using the same on-line displacement-control algorithm just described.

SEISMIC LOAD TESTING OF FIVE-STORY BUILDING

The seismic-load-simulation test program for the TCCMAR full-scale five-story research building consisted of 75 shakedown, stiffness, GSD, and ITL tests, conducted over a two-month time period. To demonstrate the effectiveness of the seismic-load simulations, representative test results from the initial test phase are presented first, followed by complete GSD and ITL response records. For the on-line test control, two sets of analog displacement transducers were used at each of the 10 structural control locations, (see Fig. 3), to measure the actual structure displacements relative to an external reference frame: one for high resolution at small displacements and the other for large-displacement measurements. During the initial or stiff behavior state of the research building, linear potentiometers with ± 25.4 mm (± 1 in.) range and 3×10^{-3} mm (0.12×10^{-3} in.) resolution were used; and on-line displacement control past the yield limit state was obtained by use of linear potentiometers with ranges as large as ± 229 mm (± 9 in.) with 27.4×10^{-3} mm (1.08×10^{-3} in.) resolution. The control-displacement accuracy at the level of indicated resolution was achieved by sampling and averaging 100 data points for each on-line displacement measurement.

Shakedown Tests and Stiffness Measurements

Following the test simulations using a five-story flexible steel frame, the 10 actuators were connected to the research building and 30 low-force level on-line simulations were conducted to test all aspects of the developed control algorithms. The shakedown tests were designed to define and fine-tune critical test parameters such as time step, displacement-error tolerance, displacement convergence, torsion control factors, and various flexibility/stiffness measurement schemes, with feedback from the actual test structure. In particular, the choice at the time step Δt for the pseudodynamic load simulation was of interest since it was no longer controlled by the (implicit) time integration scheme but rather by the highest mode response to be

captured during the test. Shakedown test stiffness measurements and analytical predictions showed (see Table 2), that in order to describe one cycle of the second mode with 10 data points, a time step of $\Delta t = 0.005$ sec was required, resulting in only five data points/cycle for the third mode, and clearly insufficient resolution to capture fourth- and fifth-mode responses. To demonstrate second and third mode response at a time step of $\Delta t = 0.005$ sec, on-line shakedown tests with prescribed increasing sinusoidal second- and third-mode displacement patterns were performed without any numerical damping in the control algorithms. Displacement and load traces in Figs. 7(*a* and *b*) show the analytical and experimental response to an increasing sinusoidal second-mode displacement input with good definition in both shape and magnitude. Similar third-mode simulation tests showed that third-mode traces can be captured experimentally at the 0.005-sec time step, [see Fig. 7(*c*)]. Thus the 0.005-sec time step was selected for the initial GSD tests and 0.01 sec for later tests allowing for possible second-mode and limited third-mode response contributions.

A complete overview of stiffness measurements and stiffness degradation throughout the test program is presented in Table 2 by means of modal dynamic response characteristics. Modal stiffness measurements as described earlier were found to be advantageous compared to conventional flexibility measurements, since larger deformations in the lower modes could be applied without exceeding tight interstory-shear-force limits. The experimentally obtained dynamic-response characteristics from prescribed low-level modal-displacement patterns show close agreement with analytical pretest predictions, as shown in Table 2. Subsequent stiffness degradation occurred primarily in the first and second modes. The first-mode degradation was also confirmed by pre- and posttest frequency sweep forced-vibration evaluations (see Table 2).

The measured stiffness matrix was used for the subsequent GSD and ITL tests. Results from a representative low-level GSD test during the shakedown test phase are shown in Fig. 8. Analytical and experimental displacement and restoring-force time histories are shown in Figs. 8(*a* and *b*), respectively, for a 0.5-sec input window from the Pine Union School ground motion recorded during the 1979 Imperial Valley earthquake. Both displacement and restoring force traces show good agreement at all five levels in shape and magnitude between the analytical prediction and the experiment, demonstrating the effectiveness of the GSD procedure to accurately capture the dynamic response of stiff multidegree-of-freedom structures by means of a pseudodynamic test.

TABLE 2. Stiffness Degradation of Five-Story Test Building

Mode (1)	Linear elastic finite-element method prediction (2)	Pretest forced vibration (3)	Shakedown test 0.002% drift (4)	Cracking limit state 0.029% drift (5)	Yield limit state 0.20% drift (6)	Ultimate limit state 1.45% drift (7)	Posttest forced vibration (8)
1	0.203	0.231[a]	0.209	0.223	0.322	0.577	0.500[a]
2	0.053	—	0.058	0.059	0.069	0.130	—
3	0.026	—	0.026	0.028	0.031	0.047	—
4	0.019	—	0.109	0.019	0.020	0.034	—
5	0.016	—	0.016	0.013	0.015	0.020	—

[a]Mixed translation and torsional mode.

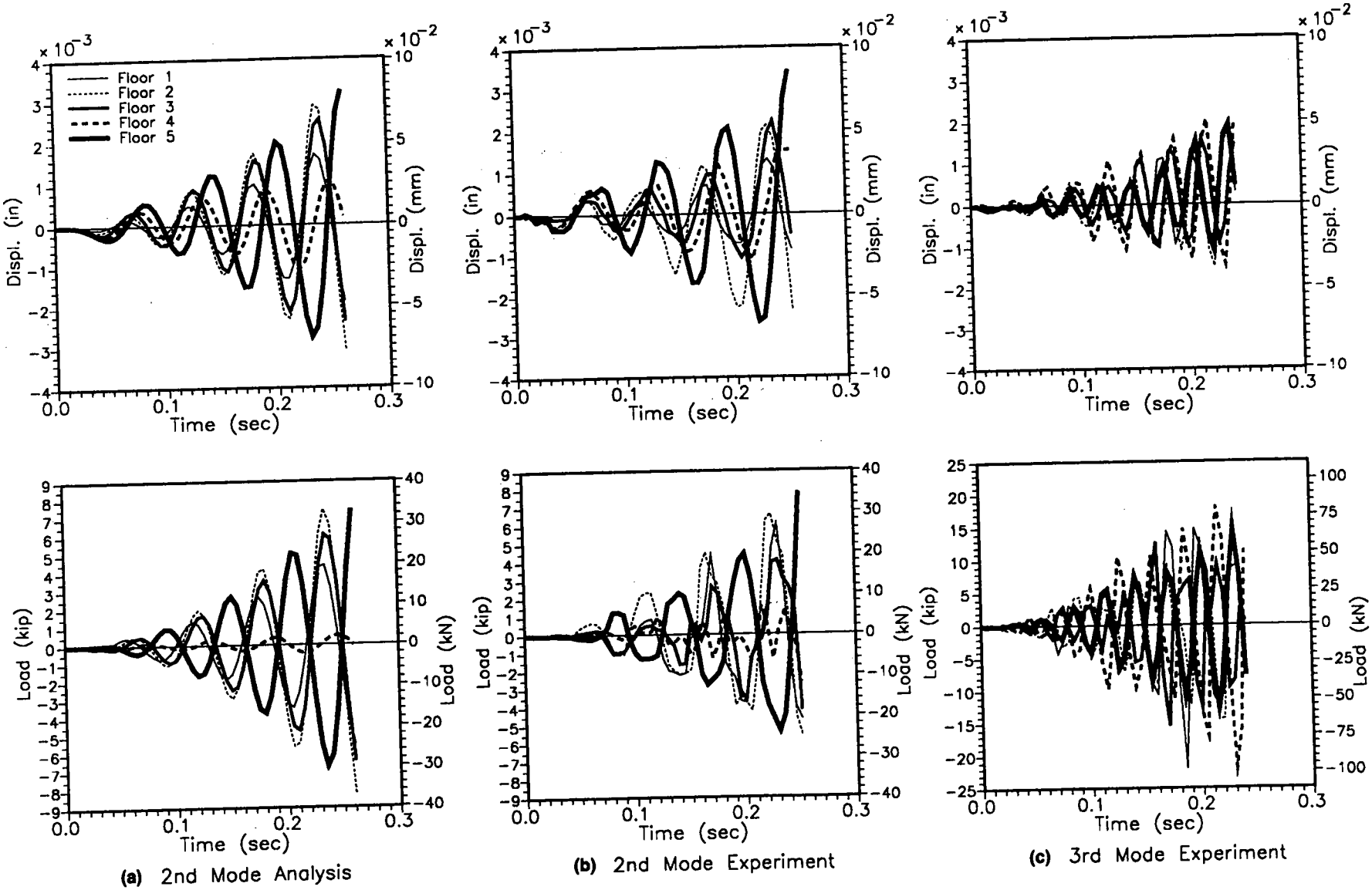

FIG. 7. Higher Mode On-Line Simulation Tests

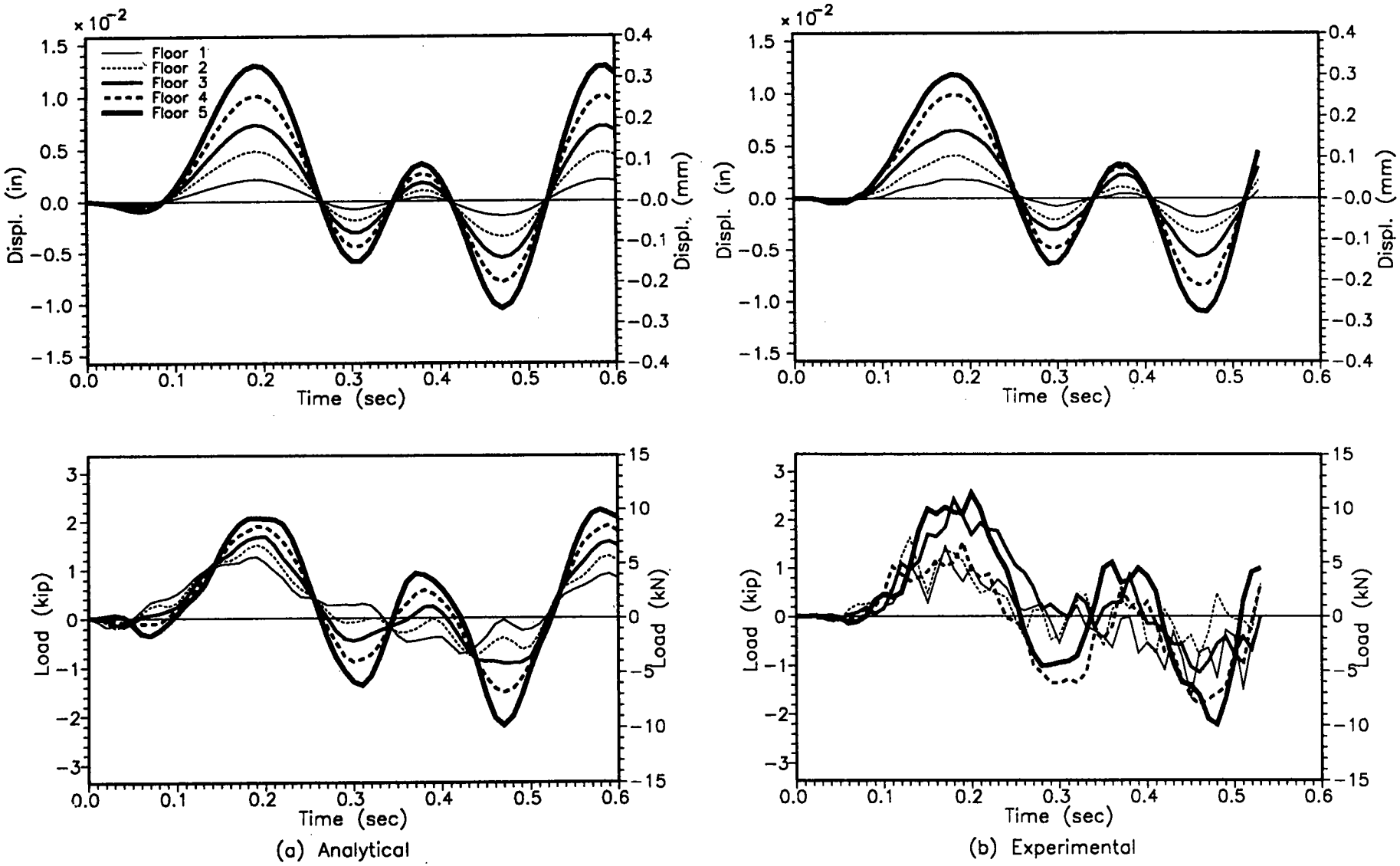

FIG. 8. Shakedown GSD Test No. 11, Pine Union School

GSD Seismic Load Simulation Tests

The core-test sequence for the five-story building comprised 15 GSD experiments (see Table 1 and Fig. 4). All structural damage was inflicted to the research building during these seismic-load simulations. Results from these tests are described by two representative GSD tests, namely test 39 at the postcracking behavior state, and test 61 at the yield limit state of the research building. Both tests represent the response to windows from recorded earthquake ground-motion traces during the 1979 Imperial Valley earthquake as shown in Table 1.

During the initial tests with little damage to the structure, e.g. test 39, the experimental displacement-time-history response agreed very well with the analytical prediction, both using the same measured pretest stiffness matrix. The displacement time history shows predominantly first-mode response [Fig. 9(*b*)]; and the restoring-force time history [Fig. 9(*c*)], clearly shows second-mode contributions, an effect that was also observed in post-test analytical simulations. The displacement-error time history [Fig. 9(*d*)], shows that the displacement error typically remained below ± 0.05 mm (± 0.002 in.). The number of inner-loop iterations was limited to seven in case the displacement error tolerance of 0.013 mm (0.0005 in.) was not reached, at which time the remaining displacement error was recorded and a restoring force correction applied in the next outer-loop step.

At the yield limit state, represented approximately by test 61, expected discrepancies between linear elastic analytical predictions and test results in the form of period elongation were recorded [see Fig. 10(*b*)]. Amplitudes did not necessarily increase due to increased hysteretic damping in the test structure with increasing damage. The restoring-force time-history [Fig. 10(*c*)] again shows the higher-mode effects, which correspond closely to those obtained from the analytical model after $t = 1.5$ sec; and from 0 to 1.5 sec, experimental restoring-force oscillations, particularly in floor five, were more pronounced than those predicted analytically. These spurious higher-mode effects at the upper floors were indicative of torsional mode control problems, and could be eliminated by relaxing the strict no-torsion compliance with a discrete torsion filter, allowing limited interstory rotations. The displacement-error time-history [Fig. 10(*d*)] shows an increased displacement error due to the less-sensitive control-displacement transducers, but falls generally well within a band of ± 0.13 mm (± 0.005 in.), with error peaks at peak structural displacements. Similar response characteristics were recorded for all other GSD tests, demonstrating good control of the test specimen with the developed GSD algorithm and the available 10-actuator servocontrol hardware.

To deduce design information directly from GSD seismic-response data is not always a simple procedure, as can be seen from Fig. 11, where a typical design-response quantity, namely the base shear, is plotted with respect to the top of the building displacement. Higher-mode effects change the ratio of overturning moment to base shear, or, in other words, the lateral force distribution pattern. To obtain the desired design information, either a lateral-load-distribution filter can be used on the GSD data (Seible et al. 1994), or, as outlined earlier, a test with a fixed lateral-load distribution pattern, e.g. inverse triangular, can be applied within the previously achieved building drift limit. The hysteresis loops from these ITL tests are depicted in Fig. 12, showing the overall ductile response of the five-story reinforced-masonry research building. As is discussed in detail in the companion paper on the seismic response of the five-story research building (Seible et al.

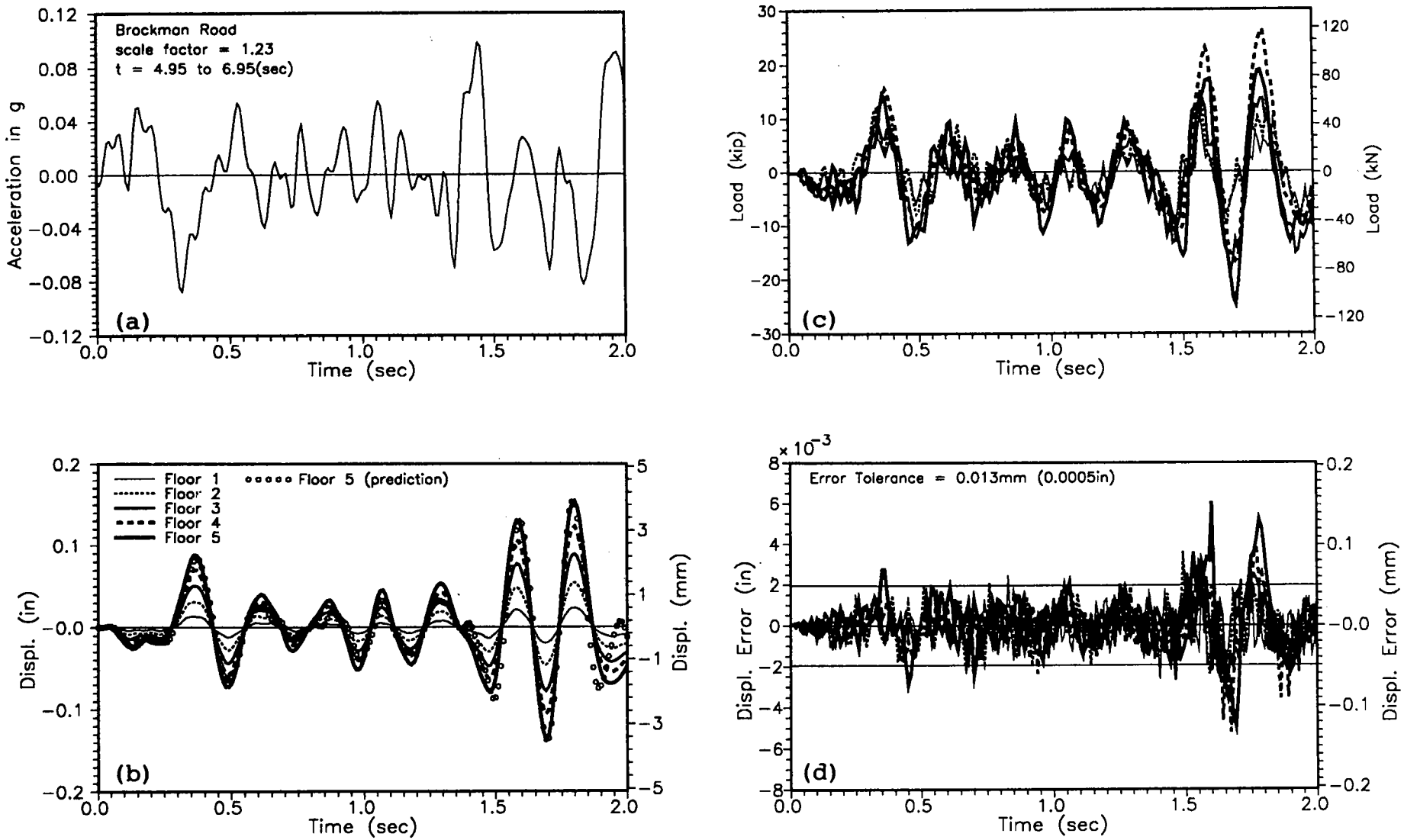

FIG. 9. GSD Test No. 39, Brockman Road

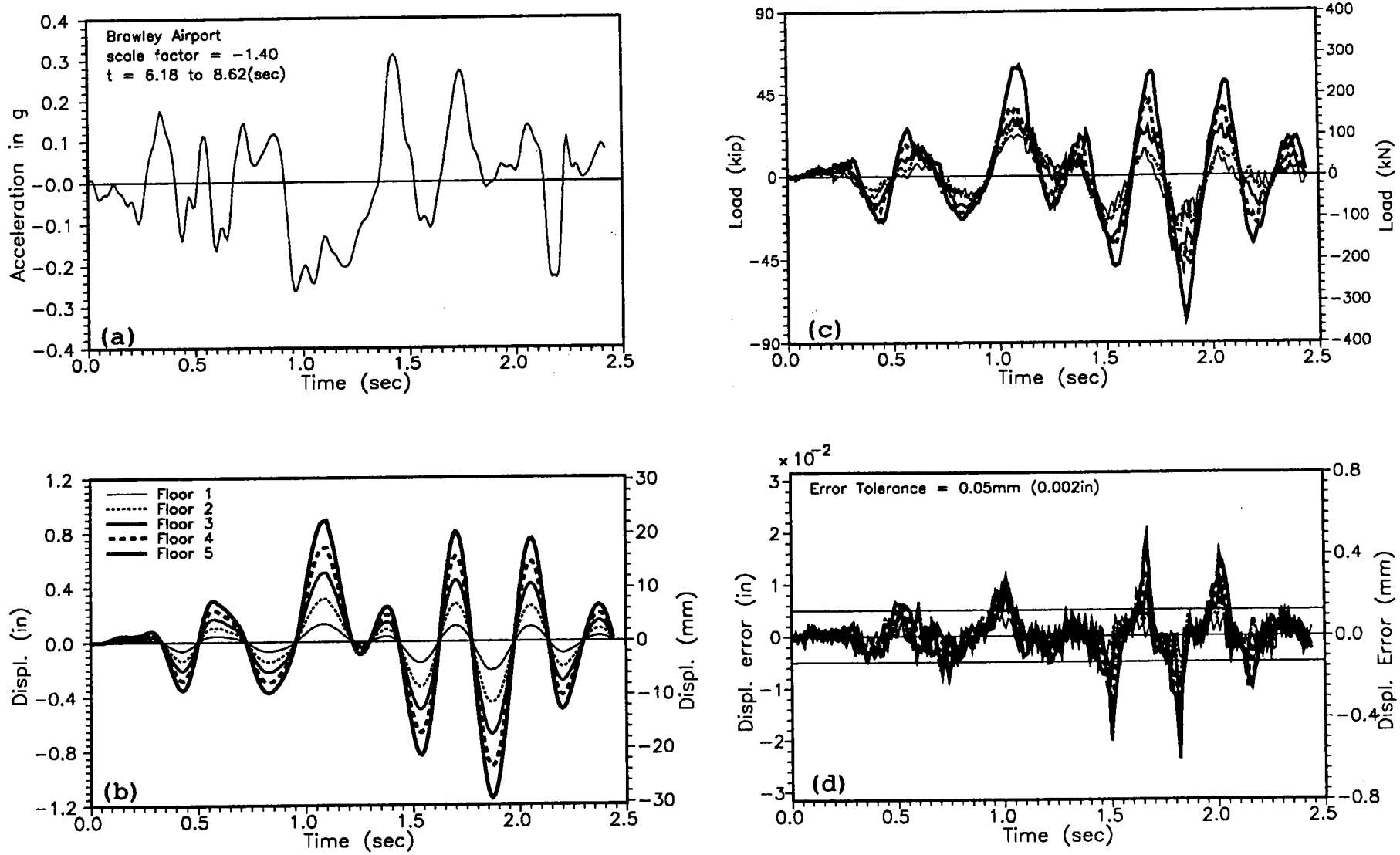

FIG. 10. GSD Test No. 61, Brawley Airport

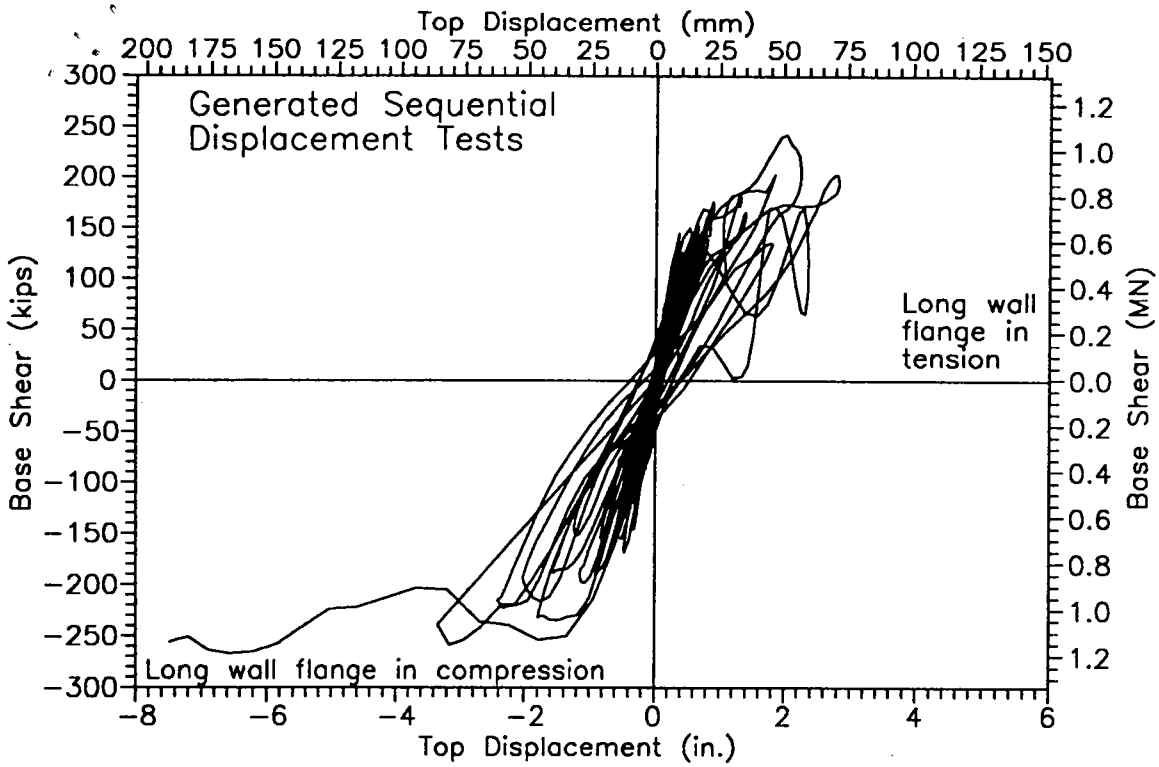

FIG. 11. Combined Base Shear versus Top Displacement Response from GSD Tests

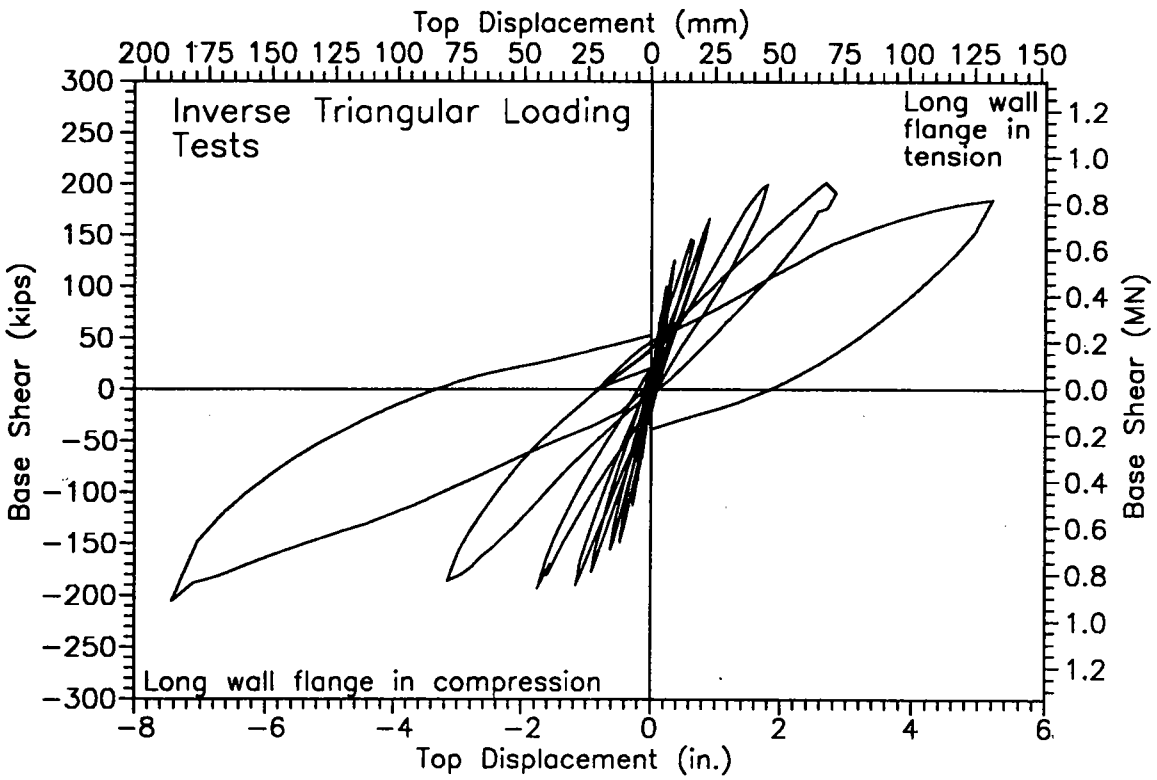

FIG. 12. Combined Base Shear versus Top Displacement Response from ITL tests

on the seismic response of the five-story research building (Seible et al. 1994) the load-deformation characteristics observed during the seismic-load-simulation tests indicate displacement-ductility levels of 6 and 9 in the two loading directions. The hysteresis loops from the ITL tests also provide information on the hysteretic energy dissipated during a fully reversed cycle, which can be converted to equivalent viscous-damping coefficients. The equivalent viscous-damping ratios obtained from the ITL tests ranged from

0.6% after the aforementioned test 39 to 4% after the yield limit test 61 and to 13.3% in the final ITL test. In summary, both GSD and ITL test algorithms were successful in both the seismic-load-simulation testing of the five-story research building and the deduction of essential design data for design model verification [see Seible et al. (1994)].

Limitations of Test Method

The soft coupling of the actuator system and the test structure by means of elastomeric pads that allowed the pseudodynamic testing of the stiff MDOF building was provided by a friction connection with highly nonlinear characteristics and even slip at higher load levels, which resulted in an increased number of iterations and overall slower test speeds. Thus, seismic strain-rate effects cannot be captured and time-dependent effects such as creep and relaxation during the test even though minimized through continuous loading and multistep ramping are present with an achieved pseudodynamic to real-time scale of approximately 2,000. For highly nonlinear structures, an increase in test speed could be achieved through improvements to the control algorithm for the implicit integration scheme: the initial stiffness matrix used to compute the target displacement in each inner loop cycle could be replaced by a continuously updated tangent stiffness matrix. Furthermore, actual structural control-displacement measurements are still the essential component for a successful pseudodynamic time and require for stiff structural systems high-resolution displacement transducers and a reliable reference frame. During the early GSD tests on the five-story masonry building, when very small displacement increments were required, temperature variations during GSD segments caused distortions in the reference frame and a drift in displacement measurements, which required all tests to be conducted at night to minimize these adverse effects.

CONCLUSIONS

The first U.S. full-scale five-story building test showed that simulated-seismic-load tests can be successfully performed under laboratory conditions using pseudodynamic testing principles. Improvements to conventional pseudodynamic tests were implemented in the soft coupling between the loading system and the test structure by means of elastomeric pads, the use of an implicit time-integration scheme with restoring-force corrections and target displacement updates, the introduction of a modal convergence and scaling procedure in the inner loop control algorithm, and the use of a torsion filter to control excessive torsion-mode effects on the restoring forces. These modifications to the control side combined with a selected sequence of earthquake-ground-motion time histories for response evaluation at characteristic design limit states form the basis for the presented GSD procedure, which was utilized to impose all structural damage to the research building. The GSD procedure allowed for limited testing of higher-mode effects. The on-line control modifications also allowed for the application of an inverse triangular load distribution pattern to obtain valuable design information from the five-story research building test. The described test represents the first full-scale test of a stiff full-scale multidegree-of-freedom structural-wall-type bulding under simulated seismic loads from the initial undamaged structural state to the maximum displacement limit state. The developed on-line test control algorithms provided the basis for the full-scale five-story RM building test to verify and fine tune new TCCMAR analysis and design models for masonry buildings in seismic zones.

ACKNOWLEDGMENTS

This first full-scale five-story seismic building test in the United States was made possible by the collaboration, support, and help of many dedicated individuals, agencies, and industry groups, with primary funding provided by research grants from the National Science Foundation, and funds from the Department of Energy. Support was also provided by the masonry industry, in particular the Masonry Institute of America, the National Concrete Masonry Association, and the Concrete Masonry Association of California and Nevada.

APPENDIX I. REFERENCES

Igarashi, A., Seible, F., and Hegemier, G. A. (1992). "Testing of full-scale shear wall structures under seismic load." *Proc., 10th World Conf. on Earthquake Engrg.*, 2653–2758.

Igarashi, A. (1993). "On-line computer controlled testing of stiff multi-degree of freedom structural sytems under simulated seismic loads," PhD Dissertation, Dept. of AMES, Univ. of California, San Diego, Calif.

Mahin, S. A., Shing, P. B., Thewalt, C. R., and Hanson, R. D. (1989). "Pseudodynamic test method—current status and future directions." *J. Struct. Engrg.*, ASCE, 115(8), 2113–2128.

Noland, J. L. (1990). "1990 status report: U.S. Coordinated Program for Masonry Building Research." *Proc., 5th North Am. Masonry Conf.; Vol. 1*, 57–68.

Paulay, T., and Priestley, M. J. N. (1992). *Seismic design of reinforced concrete and masonry structures*. John Wiley and Sons, New York, N.Y.

Porter, M. L. (1987). "Sequential phased displacement (SPD) procedure for TCCMAR testing." *Proc., 3rd Meeting*, Joint Technical Coordinating Committee on Masonry Research (TCCMAR), Tomamu, Japan.

Seible, F., Priestley, M. J. N., Kingsley, G. R., and Kurkchubasche, A. G. (1994). "Seismic response of a full-scale five-story reinforced-masonry building." *J. Struct. Engrg.*, ASCE, 120(3), 925–946.

Shing, P. B., Vannan, M. T., and Carter, E. (1991). "Implicit time integration for pseudodynamic tests." *Earthquake Engrg. and Struct. Dynamics*, Vol. 20, 551–576.

Takanashi, K., and Nakashima, M. (1987). "Japanese activities on on-line testing." *J. Engrg. Mech.*, ASCE, 113(7), 1014–1032.

APPENDIX II. NOTATION

The following symbols are used in this paper:

$\mathbf{A}$ = transformation matrix for target displacements ($n_s \times n$);
$\mathbf{A}^+$ = pseudoinverse of matrix $\mathbf{A}$;
$\mathbf{a}(i)$ = acceleration vector at the time step i;
$\mathbf{C}$ = damping matrix ($n \times n$);
$\mathbf{e}_n$ = unit vector specifying top-floor DOF;
$\mathbf{f}(i)$ = excitation-force vector at time step i;
i = time step;
$\hat{\mathbf{K}}$ = measured stiffness matrix ($n \times n$);
k = iteration step;
$\mathbf{M}$ = mass matrix ($n \times n$);
$\mathbf{N}$ = actuator-displacement-scaling matrix ($n_s \times n_s$);
$\mathbf{N}_d$ = scaling matrix for translational displacements ($n_s \times n_s$);
$\mathbf{N}_r$ = scaling matrix for rotational displacements ($n_s \times n_s$);

n = number of reduced DOF = 5;
n_s = number of structural DOF = 10;
$\mathbf{P}$ = torsion filtering matrix ($n_s \times n_s$);
$\mathbf{R}_d$ = a factor in scaling matrix ($n_s \times n_s$);
$\mathbf{r}(i)$ = restoring-force vector at time step i;
$\hat{\mathbf{r}}^{(k)}$ = measured restoring-force vector at iteration step k;
$\hat{\mathbf{r}}_S^{(k)}$ = measured structural restoring-force vector at iteration step k;
$\mathbf{u}$ = inverse triangular load pattern vector;
$\mathbf{v}(i)$ = velocity vector at time step i;
$\mathbf{x}(i)$ = displacement vector at time step i;
$\hat{\mathbf{x}}^{(k)}$ = measured displacement vector at iteration step k;
$\mathbf{x}_a^{(k)}$ = actuator displacement vector at iteration step k;
$\hat{\mathbf{x}}_S^{(k)}$ = measured structural displacement vector at iteration step k;
$\mathbf{x}_{S\text{target}}$ = structural target displacement vector;
$\mathbf{x}_{S\text{target}}^{(k)}$ = structural target displacement vector at iteration step k;
$\mathbf{x}_{\text{target}}$ = target displacement vector;
x_{top} = specified top-floor displacement for inverse triangular loading;
α, β, γ = scalar integration constants;
$\alpha^{(k)}$ = factor of proportionality to inverse triangular load pattern;
Δt = integration time interval;
κ_p = convergence controlling parameter; and
ν = global scaling factor.